Traffic Management in HSDPA via GEO Satellite

Giovanni Giambene[◇,*], Samuele Giannetti[◇],
Cristina Párraga Niebla[†], Michal Ries[‡], Aduwati Sali[♮]

[◇]University of Siena, Via Roma 56, I-53100 Siena, Italy
[†]German Aerospace Center (DLR), P.O. Box 11 16, D-82230 Wessling, Germany
[‡]University of Technology Vienna, Gusshausstrasse 25/389, A-1040 Vienna, Austria
[♮]University of Surrey, Guildford, Surrey GU2 7XH, United Kingdom

Abstract

Satellite systems are a valid alternative to cover wide areas on the earth and to provide broadband communications to mobile and fixed users. Satellite systems should be able to provide to mobile users the same access characteristics of the terrestrial counterparts. This paper investigates packet scheduling aspects for *Satellite Universal Mobile Telecommunication System* (S-UMTS) transmissions based on *Satellite - High Speed Downlink Packet Access* (S-HSDPA). A geostationary bent-pipe satellite has been considered. The performance of different scheduling schemes has been compared in the envisaged S-HSDPA scenario, considering video streaming and Web traffic flows. We have obtained that the *Proportional Fairness* scheduler with *Exponential Rule* (PF-ER) permits to achieve the best performance for video traffic. Moreover, video traffic traces have been used to evaluate the objective video quality achieved at the application layer, considering the

[*]Correspondence to: G. Giambene (e-mail: giambene@unisi.it). This paper only in part derives from a paper presented by these authors at the IWSSC 2006 conference, September 14-15, 2006, Leganés, Spain.

physical medium behavior and different S-HSDPA scheduling schemes.

Key words: *Satellite Communications*, *Scheduling*, *HSDPA*.

1 Introduction

Satellite communications deserve the special merit to allow connecting people at great distances by using the same broadband communication system and technology. Three broad sectors where satellites can be employed are: fixed satellite service, broadcast satellite service and mobile satellite service. The current interest on satellite communications is related to their capability to integrate with terrestrial networks and to have commonalities in the air interface with cellular communication systems. A particular interest is here deserved to *third generation* (3G) mobile networks and their current evolution represented by *High Speed Downlink Packet Access* (HSDPA).

HSDPA is a cost-efficient upgrade of 3G terrestrial cellular systems that delivers performance comparable to today's wireless local area network services, but with the added benefit of wide-scale mobility. HSDPA's improved spectrum efficiency enables much faster downstream throughput than today's *Universal Mobile Telecommunications System* (UMTS), giving users downlink speeds typically in the range 1 - 5 Mbit/s. Hence, capacity-demanding applications are possible for mobile users, such as video streaming.

Some of the HSDPA features that allow high bit-rates are the adoption of *Adaptive Coding and Modulation* (ACM) and the multi-code operation depending on the channel conditions (forward link) that are feed back by the *User Equipment* (UE) to the resource manager [1]–[3].

In this paper, the interest is on the proposal for the extension of HSDPA to the satellite scenario (*Satellite-HSDPA*, S-HSDPA, as an evolution of

Satellite-UMTS, S-UMTS) based on a *geostationary* (GEO) bent-pipe satellite in order to support broadband multimedia applications for mobile users. Current standardization of S-UMTS is progressing in the related working group within the ETSI *Technical Committee on Satellite Earth Stations and Systems*. S-UMTS is expected to complement *Terrestrial* UMTS (T-UMTS) and interwork with other *International Mobile Telecommunications 2000* (IMT-2000) family members through the UMTS core network. The S-UMTS Family G specification set aims at achieving the satellite air interface fully compatible with T-UMTS-based systems, even if some modifications are needed due to the differences between terrestrial and satellite channels [4]–[7].

In HSDPA, the application of ACM, dependent on the channel conditions experienced by the UE in the forward link, requires the exchange of channel state information between UE and the resource manager (scheduler) at the base station. Due to the inherently longer propagation delays in the satellite scenario, the channel state information used by the scheduler is outdated. Therefore, this paper aims at investigating the performance of different scheduling techniques for S-HSDPA by applying ACM on the basis of a non-accurate knowledge of the channel state due to the round-trip delays. Some initial considerations will be also provided for what concerns the impact of channel estimation on system capacity. This paper is an extension of the work made in [8], where the channel behavior was simply modeled as a GOOD-BAD Markov process. The interest of this work is to compare different S-HSDPA scheduling solutions in a realistic scenario for what concerns channel behavior and application traffic characteristics. In particular, we employ channel traces suitable for S-UMTS and we introduce an analytical model to investigate the impact of the channel behavior on the packet error rate, the performance of different scheduling schemes and the quality at the application level.

This paper is organized as follows. Section 2 deals with the descrip-

tion of the envisaged S-HSDPA scenario including channel characteristics, *physical* (PHY) layer and *Medium Access Control* (MAC) layer. Section 3 focuses on resource management issues, while Section 4 describes the compared scheduling schemes. Section 5 presents performance results obtained from simulations to compare the behavior of different scheduling schemes. Section 6 provides results concerning the objective video quality at the application layer. Finally, Section 7 concludes this paper highlighting further research areas.

2 Envisaged S-HSDPA Scenario

The terrestrial HSDPA architecture is not fully applicable to the satellite scenario. Firstly, in S-UMTS the location of the different network entities, such as Node-B (i.e., the base station) and *Radio Network Controller* (RNC) is not uniquely determined. Depending on the available complexity on the satellite (with or without on-board processing), part of the functionalities typically located at the Node-B (e.g., packet scheduler) or at the RNC can be executed on board or not. The fast adaptation to channel conditions that are possible in terrestrial HSDPA are partially based on the proximity between UE and scheduling entity, i.e., Node-B. In this paper, a multi-beam GEO bent-pipe satellite is considered. All *Radio Access Network* (RAN) functionalities corresponding to the network part are located at the Gateway, as shown in Figure 1. The Node-B is on the earth, close to the Gateway station. In this case, the high *Round-Trip Propagation Delay* (RTPD) value partly reduces the benefits of adaptation; this aspect will be addressed in this paper and results will be shown in Section 5.

In the following sub-Sections, we describe the radio channel characteristics as well as PHY and MAC layers of S-HSDPA.

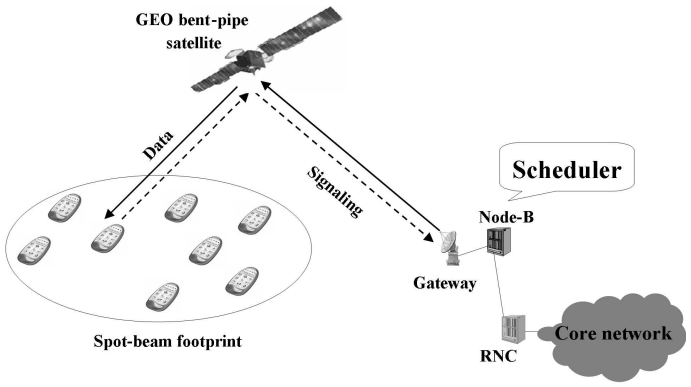

Figure 1: Envisaged S-HSDPA network architecture.

2.1 Channel Characteristics

The simulations of the S-UMTS channel model, generating *Signal-to-Noise and Interference Ratio* (SNIR) traces, are conducted representing an actual small-area propagation model at about 2 GHz, assuming an omni-directional antenna at the UE [9]. The propagation parameters of the channel are obtained from measurements, conducted at 29° elevation angle with a GEO satellite, taking place in a suburban area where both line-of-sight conditions and shadowed ones are present. In particular, it has been considered an open-space section occasionally bordered by widespread trees on both sides. Such route runs through a rural town section with one big roundabout and houses not taller than two-storeys.

To simulate this environment, a Vehicular Type A mobility at 3 km/h has been considered for the UE. The channel properties are assumed quasi-stationary for short time periods, and during these periods are represented by stationary stochastic processes. A semi-Markov model is developed, which alternates between two states: open (non-fade) and shadowed (fade) areas. The state sojourn time follows a power law distribution for non-fade duration and a lognormal distribution for fade duration. These chosen dis-

tributions are proven in [9] to allow a better representation of suburban propagation environments for land mobile satellite applications. This is especially crucial when estimating system availability and outage durations.

The channel model simulator inputs the specified open or shadowed parameters from [9] according to the fade/non-fade duration distributions and outputs the generated SNIR considering noise and interference at system-level, which includes inter- and intra-cell interference [10]. In each simulation cycle, an arbitrary probability following a normal distribution is calculated and assigned to the UE. This probability is compared to the probability of (non)fade duration depending on the state the UE is currently in. If the arbitrary probability is higher, then the state is switched. The state sojourn times are recommended parameters to match the extracted time-series parameters from measurements. For the studies carried out in this paper, a channel trace of 655 s has been obtained. Every 10 ms, the state duration is observed and SNIR is calculated accordingly. During the interval [0, 0.1 s], SNIR values oscillate from 3.8 to 4.5 dB, corresponding to a UE entering a shadowed environment in a lightly wooded areas. The signal in this area is largely influenced by shadowing due to trees foliage. In the interval [0.1, 30 s], SNIR is quite high, between 4 dB and 6.5 dB, thus corresponding to a situation with a UE in an open area. In the last interval [30, 655 s], the UE signal fluctuates from 2.5 dB to 6.5 dB; this situation corresponds to a UE in a housing area where the high fluctuations are due to the larger size of obstacles, i.e., houses, and the oscillation is because the houses are further apart with open spaces between them.

Figure 2 provides the SNIR distribution obtained from channel traces. From this figure a high probability is observed for SNIR $\sim$ 6.5 dB, because the non-fade duration (representing the open state in the envisaged suburban environment) is longer than that of the shadowed state. This is in contrast to the scattering components for lower SNIR values, which are due to the shorter fade duration of the shadowed state. The distribution of SNIR

in-between the two states is due to the transition from one state to another where the SNIR values could fall in-between.

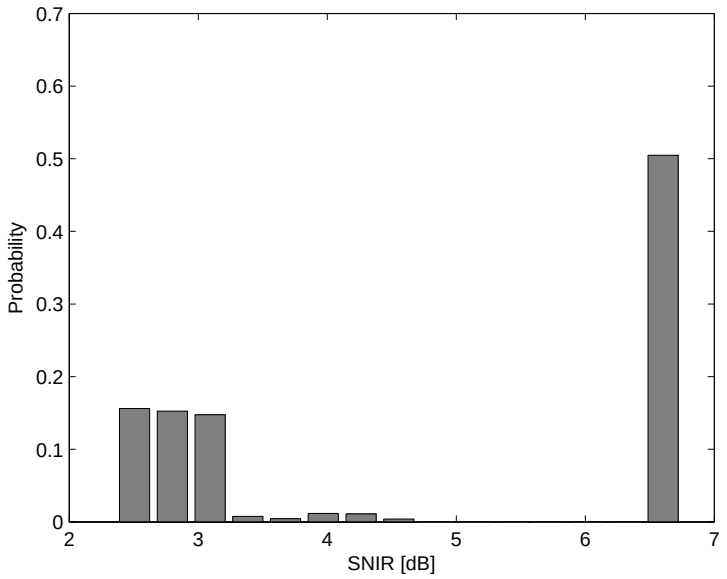

Figure 2: SNIR distribution derived from channel traces.

2.2 Physical Layer

Two fundamental W-CDMA (*Wideband-Code Division Multiple Access*) features are disabled in HSDPA, i.e., fast power control and *Variable Spreading Factor* (VSF), being replaced by ACM, multi-code operation, and *Fast L1 Hybrid ARQ* (FL1-HARQ). HSDPA uses a fixed spreading factor equal to 16 (i.e., 16 codes are available for simultaneous downlink transmissions). HSDPA is based on a sort of hybrid time-division/code-division multiplexing air interface, where packet scheduling can be done in two dimensions: time and code. The system operates in time multiplexing in essence, but during each time slot, code multiplexing is used according to two different

possible approaches, *multi-code operation* and *user-multiplexing*, as detailed below.

The *Transmission Time Interval* (TTI) is the time interval according to which codes and modulation scheme are assigned to UE(s) for data transmission. Using the multi-code operation, the throughput of one UE can be improved on a TTI basis by allocating several codes to it. Whereas, by means of user-multiplexing, several UE's can be scheduled in the same TTI, thus enhancing the resource utilization. The fixed spreading factor allows the allocation of up to 15 codes for UE traffic in each TTI (the 16-th code is only used for signaling purposes). The TTI duration can be selected on the basis of the traffic type and the number of UE's in steps of 2 ms. In comparison with the typically longer TTI's of W-CDMA (10, 20 or 40 ms), the shorter TTI duration in HSDPA allows lower delays between packets, a finer granularity in packet scheduling, multiple retransmissions, faster channel adaptation and minimal wasted bandwidth. In this paper, we will use TTI = 2 ms.

The adaptability in HSDPA to physical channel conditions is based on the selection of a coding rate and a modulation scheme, for the scheduled UE's in each TTI. In particular, the HSDPA encoding scheme is based on the Release'99 rate-1/3 turbo encoding, but adds rate matching with puncturing and repetition to obtain a high resolution on the *Effective Code Rate* (ECR), ranging approximately from 1/6 to 1. To increase the peak data rates, HSDPA has added 16QAM (*16 Quadrature Amplitude Modulation*) to the existing QPSK (*Quadrature Phase Shift Keying*) modulation of Release'99.

The RNC commands the UE to report the SNIR experienced in terms of a *Channel Quality Indicator* (CQI) value. CQI is sent by the UE with a certain periodicity (in our scenario the CQI reporting interval is 40 ms) on the uplink *High Speed Dedicated Physical Control CHannel* (HS-DPCCH). Upon reception of such information, the Node-B (and in turn the scheduler)

determines which is the most suitable modulation and coding pair to be applied at the physical layer, how many orthogonal codes are used for the transmission to a UE and, hence, the number of transmitted bits per TTI (i.e., *Transport Block Size*, TBS).

2.3 Medium Access Control Layer

The HSDPA concept is based on an evolution of the W-CDMA *Downlink Shared Channel* (DSCH), denoted as *High Speed*-DSCH (HS-DSCH). HS-DSCH is a transport channel characterized by a fast channel reconfiguration time that is very efficient for bursty and high data rate traffic. TTI also denotes the time interval according to which transport channels (in our case, HS-DSCH) provide data to the corresponding physical channels; data are organized in transport blocks that require one or more codes to be transmitted in a TTI. Different TBS values are possible, depending on the adopted modulation and the number of codes used.

The HS-DSCH transport channel is mapped onto a pool of physical channels, *High Speed Physical Downlink Shared Channels* (HS-PDSCH's), i.e., codes to be shared among all the UE's on a TTI basis.

The MAC layer functionality corresponding to HS-DSCH (namely MAC-hs) is placed at the Node-B, while in the classical UMTS case, the MAC layer functionality corresponding to DSCH is located at the RNC.

2.4 Traffic Flows

In this paper, video streaming and Web downloading traffic flows have been considered to be transmitted to UE's. Referring to video streaming, which is the main application considered in this paper, the interest is in using in the satellite context the same video codecs that are employed for terrestrial 3G systems, characterized by low resolutions and low bit-rates. UE's have limited processing capabilities and power, so that the decoding of higher rate videos becomes a quite challenging task. The mandatory codec for UMTS

streaming applications is H.263 [11], with settings depending on the streaming content type and the streaming application [12]. The used resolutions are *Quarter Common Intermediate Format* (QCIF, 176×144 pixels) for cellphones, *Common Intermediate Format* (CIF, 352×288 pixels) and *Standard Interchange Format* (SIF, 320×240 pixels) for data-cards and *Personal Digital Assistants* (PDA's). It can be assumed that the maximum supported video bit-rates are 105 kbit/s for QCIF resolution and 200 kbit/s for CIF and SIF resolutions. Then, the encoded video stream is encapsulated into 3gp or mp4 file formats [13]. Clients and streaming servers shall support an IP-based network interface for the transport of session control and video data by using the *Real-Time Transport Protocol* (RTP) over *Unreliable Datagram Protocol* (UDP) over IP (see Figure 3) [13].

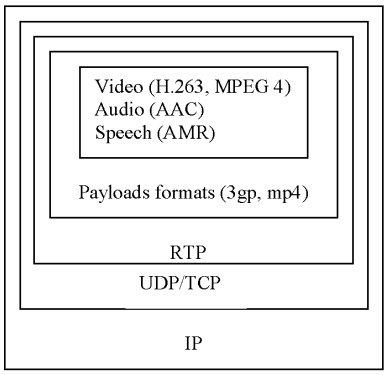

Figure 3: Overview of the video streaming protocol stack.

The video streaming services over UMTS/HSDPA in the packet-switched domain suffer from packet losses and delays that depend on the radio channel conditions. Packet loss and delay produce various kids of artifacts and their possible space and time propagation [14].

SIF and QCIF video traces have been obtained with Quicktime 7.0, according to the description made in Section 6. A discrete-time Markov chain model has been also derived through a fitting process, as described in

Section 5.

As for Web downloading traffic, we have to consider that it is an HTTP (*Hyper Text Transfer Protocol*) application based on TCP (*Transmission Control Protocol*). Due to the feedback nature of TCP-based traffic, it is more complicate to use real traffic traces in these cases, since these traces should consider the delay behavior of the system which is the subject itself of this work. To overcome these difficulties, we have generated the Web downloading traffic through a model where IP datagrams arrive according to a *Markov-Modulated Poisson Process* (MMPP) [15]. Each Web traffic source generates a bursty traffic with mean bit-rate of 5.83 kbit/s. Further details on the adopted Web traffic model are provided in Section 5.

In this paper, we will show two kinds of results: layer 3 performance evaluation and application layer objective quality. In the first case, we have studied the performance for video and Web traffic flows that have been generated according to models. In the second case, we have only used video traffic that has been generated according to traces in order to play back the received video stream, thus evaluating the resulting quality.

3 S-HSDPA Resources

All resource management functions for the envisaged S-HSDPA system are managed by the Node-B on the earth that is directly linked to the RNC that is connected to the Gateway towards the core network (see Figure 1). Several combinations of modulation and coding rates can be used on a TTI-basis for the HSDPA air interface; in the terrestrial HSDPA standard there is no defined scheduling scheme to select the UE to be served on the basis of channel conditions and traffic characteristics. This is the reason why the interest of this paper is in evaluating the performance of different scheduling techniques for the S-HSDPA proposal. The scheduler relies on received CQI information, that is the signal quality information sent by each UE. CQI provides the following information related to the transmission characteristics

currently supported by the UE in order to guarantee a minimum *BLock Error Rate* (BLER) level, $BLER_{threshold}$:

- The modulation type, that is QPSK or 16QAM;
- The number of HS-PDSCHs (i.e., codes) that can be used by the UE for its transmissions in a TTI;
- The corresponding maximum TBS value for which the $BLER_{threshold}$ requirement is fulfilled.

CQI values range from 1 to 30 with the 0 value meaning that no transmission is possible with the required maximum BLER level, $BLER_{threshold}$. Depending on the UE category, the CQI value is upper bounded by a value typically lower than 30 in order to limit the bit-rate that a UE can receive. For instance, Table 1 shows a CQI characterization that is used for some UE categories and that permits to use CQI values up to 22 (i.e., the maximum UE bit-rate is about 3.58 Mbit/s). This Table describes for each CQI value the corresponding TBS, the number of needed codes (i.e., number of HS-PDSCH) per TTI, the adopted modulation and the corresponding instantaneous bit-rate [16]. As CQI increases, so does the traffic capacity.

From Table 1 we can calculate the ECR value of each CQI according to the following formula:

$$ECR(CQI) = \frac{24 + TBS(CQI)}{l_{code} \times number\_of\_codes} \quad (1)$$

where $TBS(CQI)$ denotes the length of the transport block, 24 bits are used for the *Cyclic Redundancy Check* in HSDPA and l_{code} is the number of bits transmitted on each code in a TTI, that corresponds to 960 bits for QPSK and to 1920 bits for 16QAM.

In the terrestrial environment, the target maximum BLER is set to $BLER_{threshold} = 0.1$, since if the first transmission is unsuccessful, retransmissions are employed according to the FL1-HARQ scheme that quickly

Table 1: CQI characterization for UE categories from 1 to 6.

CQI	**TBS [bits]**	**n. of codes**	**modulation**	**UE bit-rate [kbit/s]**
0	no-Tx	no-Tx	no-Tx	no-Tx
1	137	1	QPSK	68.5
2	173	1	QPSK	86.5
3	233	1	QPSK	116.5
4	317	1	QPSK	158.5
5	377	1	QPSK	188.5
6	461	1	QPSK	230.5
7	650	2	QPSK	325
8	792	2	QPSK	396
9	931	2	QPSK	465.5
10	1262	3	QPSK	631
11	1483	3	QPSK	741.5
12	1742	3	QPSK	871
13	2279	4	QPSK	1139.5
14	2583	4	QPSK	1291.5
15	3319	5	QPSK	1659.5
16	3565	5	16QAM	1782.5
17	4189	5	16QAM	2094.5
18	4664	5	16QAM	2332
19	5287	5	16QAM	2643.5
20	5887	5	16QAM	2943.5
21	6554	5	16QAM	3277
22	7168	5	16QAM	3584

permits to recover the lost data. This approach has to be modified in our GEO satellite scenario, since RTPD (here considered equal to 560 ms) practically prevents the use of retransmissions to recover packet losses for real-time traffic. This is the reason why the transmission modes in S-HSDPA have to be selected in order to guarantee much lower $BLER_{threshold}$ values. This is a mandatory cross-layer optimization for having an acceptable video streaming quality in our GEO satellite scenario. As explained later in this Section, we have considered the requirement $BLER_{threshold} = 0.01$ instead of 0.1. Note that the high RTPD value creates a 'misalignment' between the current SNIR value at the UE and the CQI level used in the received data from the Node-B; hence, the resulting BLER value for the received data could be different (either lower or much higher) with respect to the $BLER_{threshold}$ requirement.

In [17], an analytical formula fitting the simulation experiments for the Vehicular Type A mobility environment with an RMSE (*Root Mean Square Error*) of 0.1 dB is found to relate BLER, CQI and SNIR as follows:

$$SNIR(CQI, BLER) \approx \frac{\sqrt{3}-\log_{10} CQI}{2} \log_{10}(BLER^{-0.7} - 1) + \\ + 1.03CQI - 17.3 \quad [\text{dB}]. \tag{2}$$

Considering the BLER behavior as a function of SNIR we can note that the curves obtained for two adjacent CQI values, have approximately the distance of 1 dB. Therefore, even quite small SNIR variations can have a significant impact (in the range of some orders of magnitude) on BLER for a given CQI value.

Note that formula (2) is more general than Table 1; hence, it can be also used for CQI values greater than 22. Since the UE selects the CQI value, we are interested to determine the CQI value depending on $BLER_{threshold}$ and the current SNIR value. Therefore, we need to invert the above formula (2) to express CQI as a function of SNIR and BLER (where BLER is here considered the requirement value, $BLER_{threshold}$). By operating on (2), this

formula can be expressed in the form

$$xe^x = y.$$

Unfortunately, the above expression is not invertible on the whole y domain; the inversion would require the use of the Lambert w-function, $y = lambertw(x)$. Approximated inverse functions are available in literature for some $BLER_{threshold}$ values. However, assuming CQI ≥ 1 (as it is in our case since the possible CQI values are positive and integer), the inversion is possible (i.e., there is only a solution). Hence, for a more general approach, we have numerically inverted (2) in Matlab by means of the 'fsolve' function, thus taking the integer part of the result for CQI. In case the obtained CQI value was greater than 22, we have considered CQI = 22 to be coherent with the CQI limitations in Table 1. On the basis of this numerical inversion method, for any given time t we can compute the CQI value corresponding to $SNIR(t)$ and the BLER requirement as follows:

$$CQI(t) = CQI(SNIR(t),\ BLER_{threshold}). \tag{3}$$

We can thus map the different SNIR values to the corresponding CQI ones in order to guarantee a given BLER value.

As already anticipated, the propagation delay associated to our GEO-based satellite system can generate a misalignment between the current SNIR value of the received signal at the UE and the CQI value that was used by the Node-B for the transmission to that UE. In particular, at least RTPD pass[1] from the CQI level selection to the instant when a transport block with that CQI level is received by the UE. On the basis of the channel traces that have been described in sub-Section 2.1, we have that this misalignment time entails an SNIR variation that depends on the channel status. In the worst case, we could have even an SNIR decrease of about 4.5

[1]Note that due to the selected CQI reporting interval of 40 ms, the misalignment time may grow up to a maximum of RTPD + 40 ms = 600 ms. Anyway, for the following study we will assume a fixed misalignment time equal to RTPD.

dB that could cause a very significant BLER increase. However, we could also have a SNIR increase of about 4 dB, thus entailing an inefficient use of resources due to the selection of a lower CQI value than that the system could support. Since the most harmful impact of the misalignment is that of the use of a too high CQI value with respect to the current SNIR level, a possible method to overcome this problem is that the UE selects the CQI value by considering a suitable margin h [dB] on SNIR in (3). Hence, the CQI selection is performed at the UE as follows:

$$CQI = CQI(SNIR - h,\ BLER_{threshold}). \tag{4}$$

From the above formula we can note that $BLER_{threshold}$ and h have a joint impact on the CQI determination (both $BLER_{threshold}$ reduction or h increase shift the curve of the CQI values as a function of SNIR towards higher SNIR values). Of course, the lower $BLER_{threshold}$, the lower system capacity. Our approach is to select a $BLER_{threshold}$ value (i.e., 0.01 to be conservative with respect to the terrestrial case) and then to optimize h in order to reduce the effects due to the misalignment; we will show later in this Section a method for h selection depending on the $BLER_{threshold}$ value.

The BLER at time t according to which the UE receives the transport block should take care of the misalignment time of $t - RTPD$ in the CQI selection. For this purpose, it is easy to invert (2) with respect to BLER, thus expressing $BLER(t)$ as follows:

$$\begin{aligned} BLER(t) &= BLER[SNIR(t), CQI^*(t)] = \\ &= \left[10^{2\frac{SNIR(t)-1.03CQI^*(t)+17.3}{\sqrt{3}-\log_{10} CQI^*(t)}} + 1\right]^{-\frac{1}{0.7}} \end{aligned} \tag{5}$$

where $CQI^*(t) = CQI(t - RTPD)$ is obtained from (4) with $SNIR = SNIR(t - RTPD)$ to take into account the misalignment time.

Hence, we use the above BLER formula (5) to decide in the simulations (through a probabilistic check) whether the received transport block is correct or not on the basis of the SNIR channel trace and the CQI mapping

(4).

We are interested to study the impact of the margin h value on parameter $BLER^{\mathrm{a}}$ that denotes the mean BLER value considering the average of $BLER(t)$ in (5) over all the channel trace described in sub-Section 2.1. In particular, we have:

$$BLER^{\mathrm{a}} = \int\limits_{\substack{channel \\ trace,\, t}} BLER\,(t)\, dt. \tag{6}$$

Moreover, we would like to derive the IP packet loss probability (P_{loss_IP}) due to transport block loss events for two cases ([2]):

- IP packet length distribution generated by the video source in the SIF case with mean bit-rate of 160 kbit/s and maximum IP packet length of 790 bytes.

- IP packet length distribution generated by the Web source: truncated Pareto distribution with mean value of about 479 bytes, minimum value of 81.5 bytes and maximum value of 66666 bytes. For this traffic source the maximum IP packet length is 1500 bytes.

For more details on these traffic source models, please refer to Section 5. It is interesting to note that these sources produce IP packets of different lengths from few tens of bytes up to hundreds of bytes; if a datagram is generated that is longer than the allowed maximum, it is fragmented in many IP packets. Hence, we have two alternative cases: (i) more IP packets from the same source could be accommodated in the same transport block; (ii) many transport blocks are needed to convey one IP packet.

Let l_{TB} denote the length of the current transport block size ($l_{TB} = TBS(CQI)$ according to Table 1) and l_{IP} be the IP packet length. Let us assume that the current IP packet length and transport block size are

[2]We consider here that an IP packet is lost even if any its part is lost due to errors in the related transport block transmissions.

maintained for a sufficiently long interval. We consider to have to transmit a continuous stream of IP packets to a given UE, so that partially used transport blocks by an IP packet are filled in with part of the next IP packet ([3]). Let us also consider uncorrelated losses at layer 2 (BLER level); such assumption allows for a worst case analysis from layer 3 standpoint. We can relate BLER to the P_{loss_IP} achieved at the IP level by means of the following formula (upper bound) that considers two cases, $l_{IP} \leq l_{TB}$ and $l_{IP} > l_{TB}$:

$$P_{loss\_IP}(l_{IP},\ l_{TB},\ BLER) \approx \approx \begin{cases} \dfrac{\left\lceil l_{TB}/l_{IP} \right\rceil + 1}{l_{TB}/l_{IP}} BLER & , \quad \text{for } l_{IP} \leq l_{TB} \\ 1 - (1 - BLER)^{\left\lceil l_{IP}/l_{TB} \right\rceil + 1} & , \quad \text{for } l_{IP} > l_{TB} \end{cases} \tag{7}$$

where $\lceil . \rceil$ denotes the *ceiling function*; note that the '+1' term that sums to ceiling function terms can be explained as follows:

- If $l_{IP} > l_{TB}$, the worst case is that $\left\lceil l_{IP}/l_{TB} \right\rceil + 1$ transport blocks are used to send an IP packet;
- If $l_{IP} \leq l_{TB}$, the worst case is that a transport block loss has impact on the loss of $\left\lceil l_{TB}/l_{IP} \right\rceil + 1$ IP packets.

In the case $l_{IP} > l_{TB}$, formula (7) is obtained by using the same BLER value for all the transport blocks that are needed to transmit the IP packet. Of course this is an approximation if the IP packet length is particularly long and/or the CQI level is quite low, since the different transport blocks used to send the IP packet could experience different BLER values. Also scheduling decisions could have impact on the BLER differentiation among these transport blocks.

[3] An intermediate layer is assumed to segment&reassembly the IP packets that are conveyed by different transport blocks.

From (7), we can note that $P_{loss\_IP}\left(l_{IP},\ TBS(CQI),\ BLER\right) \geq BLER$, in any case. Formula (7) highlights that P_{loss_IP} depends on the distribution of the IP packet length (that in turn depends on the traffic source, i.e., video or Web), the BLER value and, hence, the SNIR value, and the l_{TB} value due to CQI mapping. Due to the misalignment of RTPD, we need to use $BLER(t)$ given in (5) and $CQI^*(t) = CQI(t - RTPD)$ from (4). The P_{loss_IP} value can be obtained by averaging (7) over the whole channel trace and over the IP packet length distribution:

$$P_{loss\_IP} = \int\limits_{\substack{channel\\ trace,\, t}} \int\limits_{l_{IP}} P_{loss\_IP}\left[l_{IP},\ TBS\left(CQI^*\left(t\right)\right),\ BLER\left(t\right)\right] pdf\left(l_{IP}\right) dt\ dl_{IP} \tag{8}$$

where $pdf(l_{IP})$ denotes the IP packet length distribution that depends on the traffic source type; see Figure 4 below for some examples that are derived from the traffic models described in Section 5.

In Figure 5, we have evaluated BLER averaged over the whole channel trace, $BLER^{\mathrm{a}}$ as a function of the margin that is shown with negative values (i.e., $-h$) to indicate that it scales the SNIR value. Moreover, we have evaluated P_{loss_IP} according to (8) for the two IP packet length distributions in Figure 4; the *dashed curve* is for video sources and the *dash-dot curve* is for Web sources. Figure 5 also shows the capacity available for a UE averaged over the whole channel trace according to the following formula:

$$mean\ UE\ capacity = \int\limits_{\substack{channel\\ trace,\, t}} \frac{TBS\left[CQI^*\left(t\right)\right]}{TTI} dt \qquad \left[\frac{bit}{s}\right]. \tag{9}$$

It is important to select the appropriate h value and the results shown in Figure 5 can be used for this purpose. Of course the highest is the h margin value, the lowest are $BLER^{\mathrm{a}}$ and P_{loss_IP} values. However, we cannot increase the margin h value too much, otherwise the loss in capacity is evident. According to Figure 5, we can note that the adoption of a margin value h

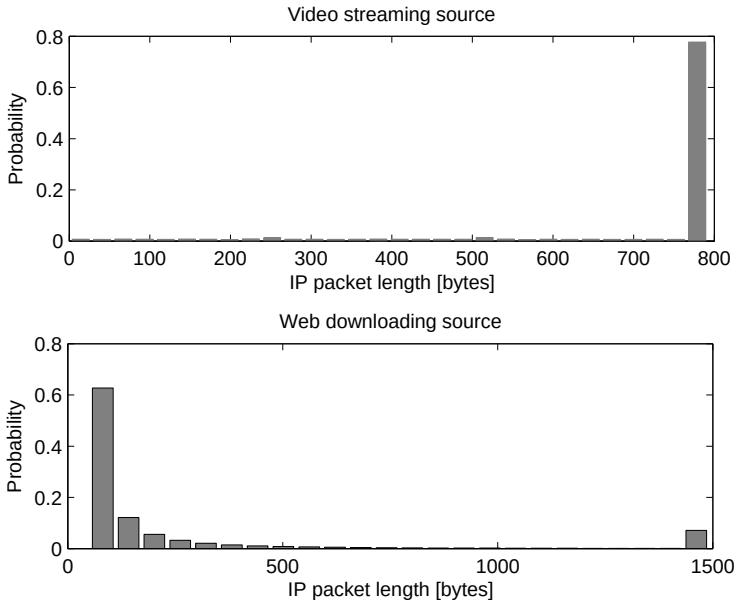

Figure 4: IP packet length distribution for both SIF video source and Web one.

around 3.5 dB is a reasonable solution since it is the lowest h value allowing $BLER^{\text{a}}$ lower than 1% (our requirement, as specified with $BLER_{threshold}$). Figure 5 in the lower part also compares the mean UE capacity as a function of the margin value with the ideal capacity we could have in the case $RTPD = 0$ with no margin (or if there could be the possibility to use an ideal channel predictor when the CQI value is selected by the UE or used at the Node-B).

Figure 6 shows the CQI* distribution obtained with the channel trace described in sub-Section 2.1 for margin values $h = 4$ dB, 3.5 dB and 0 dB (i.e., no margin); on the basis of these results, we can note that there is a significant impact of the margin h value on the CQI selection process.

Before concluding this Section it is important to point out that for S-HSDPA we have here proposed to use a different $BLER_{threshold}$ value and

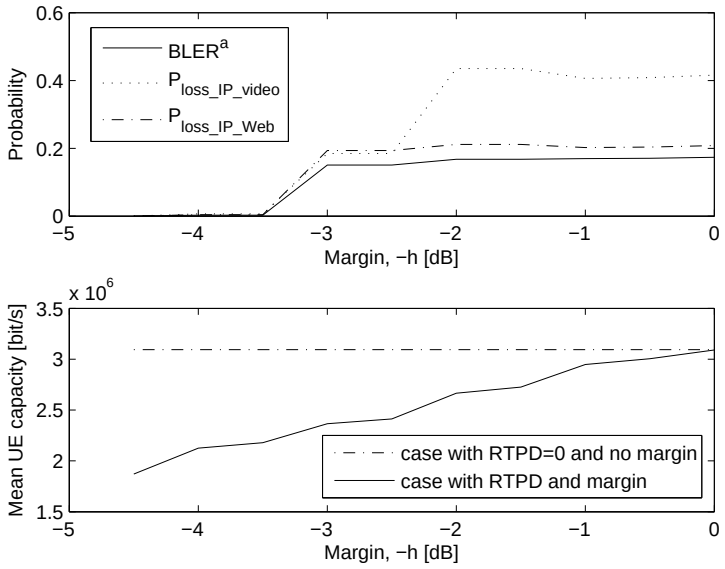

Figure 5: $BLER^{\mathrm{a}}$, P_{loss_IP} for both video and Web traffic sources ($P_{loss\_IP\_video}$ and $P_{loss\_IP\_Web}$, respectively) and *mean UE capacity* as a function of different margin values ($-h$) in dB for $BLER_{threshold} = 0.01$.

a margin in the CQI selection process, but the main characteristics of the terrestrial HSDPA remain in the aim of the maximum commonality. The requested modifications could be done in the UE's firmware (i.e., CQI selection algorithm). This could be an interesting outcome for the future proposal of the S-HSDPA standardization.

4 S-HSDPA Packet Scheduling

The envisaged applications produce traffic at the IP level for transmission via satellite. We only consider video streaming and Web traffic classes since they appear to be the most appropriate and demanding ones for our S-HSDPA scenario. For each video packet (IP level) a deadline of 160 ms is used; if the packet is not correctly transmitted within this time, it is cleared

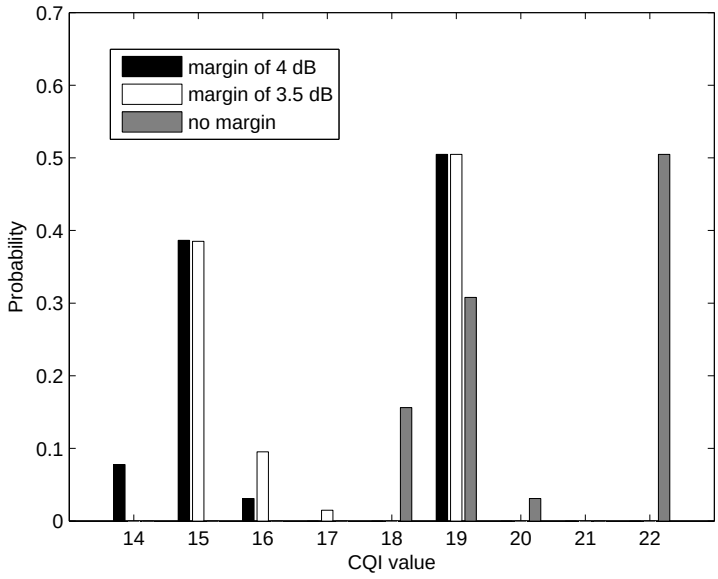

Figure 6: Resulting CQI* distribution for the use of (4) on the SNIR channel trace with 4 dB and 3.5 dB margin values compared with the no margin case.

from the layer 3 buffer, thus contributing to the packet dropping probability. We have also considered a 'virtual' deadline for IP packets generated by Web downloading of 500 ms; such deadline only indicates a preferential maximum delay for Web traffic (a Web packet exceeding its deadline is transmitted anyway).

In our study, we envisage that scheduling for the transmission at the Node-B on the HS-DSCH transport channel is performed at the level of the corresponding layer 3 IP queues, as described in Figure 7. We have distinct queues for different traffic flows (i.e., video streaming and Web downloading) according to the DiffServ approach. In each queue, the IP packets destined to different UE's are collected. Every TTI a UE is selected by the scheduler to be served and correspondingly at least one IP packet is delivered for this UE to the layer 2 HS-DSCH transmission queue (multi-code operation

mode). We employ a form of segmentation at layer 3 that also allows that part of an IP packet be included in a transport block; an intermediate layer between level 2 and 3 is in charge of segmentation and reassembly.

Recalling the previous notation of $l_{TB} = TBS(CQI)$ and l_{IP}, we have:

- If $l_{TB} > l_{IP}$, more than one IP packet (if available) for the same UE is delivered to layer 2 in a TTI with the encapsulation in transport blocks. This method allows an efficient use of resources.
- If $l_{TB} < l_{IP}$, more TTI's are employed to transmit the IP packet to the UE.

Note that the layer 2 queue for HS-DSCH is simply used as a first-input first-output transmission buffer. Such approach with layer 3 scheduling and layer 2 transmission buffer is compliant with the ETSI *Broadband Satellite Multimedia* (BSM) protocol stack and related ESA Satlab cross-layer resource management proposals [18].

We have considered and described below two alternative packet scheduling techniques, that is *Proportional Fairness* (PF) [19] and *Proportional Fairness with Exponential Rule* (PF-ER) [20]. In both cases, scheduling decisions are taken at layer 3 (i.e., UE selection for the service of its IP packet in the layer 3 queue) on the basis of urgency parameters associated to UE's that are computed according to layer 2 service parameters and layer 1 CQI information. In the next Sections, for the sake of comparison, we will also show results in the case of the *Earliest Deadline First* (EDF) scheduler that bases its decisions only on the residual lifetime of IP packets.

In the following description, we will consider that each traffic flow corresponds to a distinct UE.

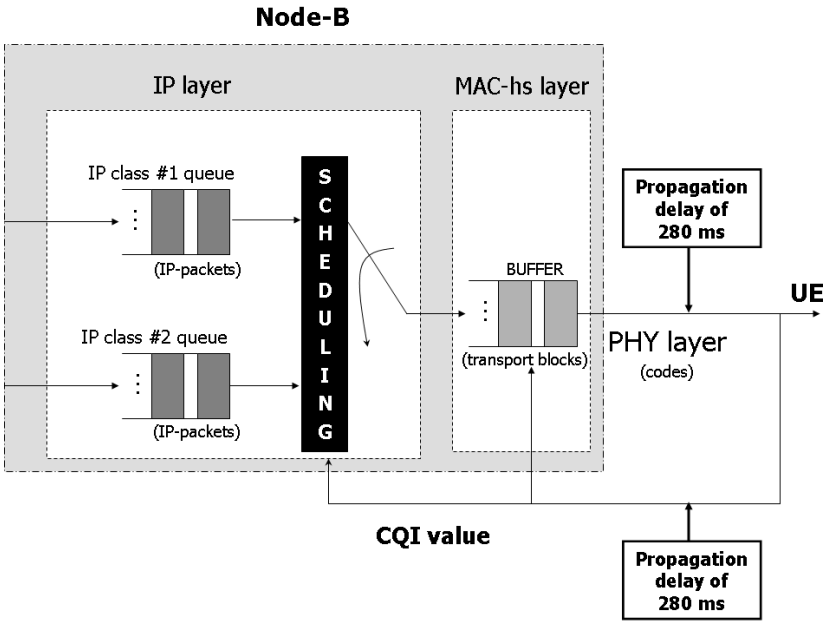

Figure 7: Resource management architecture for S-HSDPA with separate layer 3 queues for distinct traffic classes and layer 3 scheduling.

4.1 PF Scheduler

PF serves the UE with the largest *Relative Channel Quality Indicator* (RCQI), which represents the ratio between the maximum data rate currently supported by the UE (according to its CQI and the corresponding TBS) and the UE throughput averaged on a sliding window of suitable width. This approach allows a tradeoff in the service between the UE's that have better channel conditions and those that up to now have received less resources. RCQI is evaluated as:

$$RCQI_k[n] = \frac{R_k[n]}{T_k[n]} \tag{10}$$

where k is the UE index and $n = 1, 2, ...$ is related to the time measured in TTI units. Moreover, $R_k[n]$ is the maximum bit-rate supported by the k-th UE in the n-th TTI; $R_k[n]$ is calculated as the throughput that is allowed by the CQI in the next TTI interval, i.e., $R_k[n] = TBS[CQI^*[n]]/TTI$. $T_k[n]$

represents the average throughput for the k-th UE, updated every TTI in our simulations.

The limit of the PF scheduler is that it takes into account channel variations, but it does not consider the service delay. Moreover, no *Quality of Service* (QoS) differentiation is provided among traffic classes and this problem can be critical in the presence of real-time traffic.

4.2 PF-ER Scheduler

In order to introduce differentiation among different traffic classes, we have considered here the PF scheme with the variant ER, where the above RCQI index is modified by introducing a multiplicative coefficient that takes into account the transmission delay as follows:

$$ER_k[n] = RCQI_k[n] \times a_k e^{\frac{a_k w_k[n] - \overline{aw}}{1+\sqrt{\overline{aw}}}} \tag{11}$$

where:

$$a_k = \frac{-\log_{10}(\delta_k)}{T_{deadline_k}} \tag{12}$$

$$\overline{aw} = \frac{1}{N_u} \sum_{k=1}^{N_u} a_k w_k[n]. \tag{13}$$

In (11) and (13), $w_k[n]$ represents the delay (in seconds) of the oldest queued IP packet of the k-th UE (head-of-line packet for the UE). In (12), $\delta_k \in (0, 1]$ is related to the desired probability to fulfil the deadline $T_{deadline_k}$ (in seconds) [20]. In (13), N_u denotes the total number of UE's in the cell.

For the different traffic classes, the following parameters have been used:

- $\delta_k = 0.01$ and $T_{deadline_k} = 0.16$ s for video traffic;
- $\delta_k = 0.1$ and $T_{deadline_k} = 0.5$ s for Web traffic.

5 Evaluation of Performance at Layer 3

This Section describes the simulator settings and the performance results obtained with the different scheduling schemes. In our simulator, the system is modeled as described in Section 2-4. In particular, simulations have been performed for the UE's in a cell (i.e., satellite antenna spot-beam), by using the channel SNIR trace described in sub-Section 2.1 to determine the CQI value to be used at the Node-B for each transmission to the related UE. We have associated to each UE generating traffic the same channel SNIR trace, but starting it at a random instant uniformly distributed in the whole interval of 655 s and folding the trace back at the beginning when arriving to its end. The h margin value of 3.5 dB (requirement $BLER_{threshold} = 0.01$) selected in Section 3 has been used to achieve numerical results. We have made the simplifying assumption that only one UE can be scheduled (i.e., uses resources) per TTI, according to the multi-code operation mode.

In this Section, performance results are obtained in the presence of simulated video and Web traffic flows obtained with suitable models. In the next Section, performance results in terms of quality evaluation at the application level are obtained considering only video traffic provided by real video traces.

As for the video traffic, we have considered two typical UMTS video streaming scenarios [2]: (i) the "cell-phone" scenario with QCIF resolution and a mean bit-rate of 44 kbit/s (7.5 frames/s); (ii) the "PDA" scenario with SIF resolution and a mean bit-rate of 160 kbit/s (7.5 frames/s). In both cases, video frames are generated every 133 ms and fragmented in IP packets with maximum length of 790 bytes (this is the best tradeoff between RTP/UDP/IP overhead, end-to-end latency and busty error characteristics at the link layer [21]). Video traffic traces have been generated in streams of 5000 s. H.263 encoded videos were encapsulated in 3gp format by means of Quicktime 7.0; we have analyzed these traces to extract the information of the IP datagrams produced by the different video frames. On the basis

of these traces we have been able to fit a fluid flow discrete-time Markov chain model according to [22]. We have fitted mean, variance and maximum bit-rate of the video trace.

The Web traffic has been simulated by means the MMPP model shown in [15]. In particular, a Web traffic source oscillates between a *packet call* state and a *reading time* one. In the packet call state, a source produces a number of datagrams geometrically distributed with mean value 25 and the datagram interarrival time is exponentially distributed with mean value 0.5 s. In the reading time state (length exponentially distributed with mean value of 4 s) no traffic is generated. Each datagram has a length in bytes with a truncated Pareto distribution with minimum, mean and maximum values, respectively equal to 81.5, 479 and 66666 bytes. The maximum IP packet length for Web traffic has been set to 1500 bytes. The resulting mean bit-rate is of about 5.83 kbit/s.

The following performance parameters have been evaluated in this Section to compose the different scheduling techniques:

- P_{drop}, the IP packet dropping probability due to deadline expiration for video traffic sources;
- $P_{loss,\ tot}$, the total IP packet loss probability considering both the drop due to deadline expiration (only in case of video traffic), P_{drop}, and the loss due to errors introduced by the channel, P_{loss_IP};
- $Delay_{Web}$, the mean transmission delay for an IP packet produced by a Web traffic source.

With current video codecs, the maximum $P_{loss,\ tot}$ value guaranteeing an acceptable video quality is around 7%. $P_{loss,\ tot}$ and P_{loss_IP} are related as follows:

$$P_{loss,\,tot} = \begin{cases} P_{drop} + (1 - P_{drop})\, P_{loss\_IP} & , \quad \text{for video traffic} \\ P_{loss\_IP} & , \quad \text{for Web traffic.} \end{cases} \tag{14}$$

According to (14) we can find a suitable balance between P_{drop} and P_{loss_IP}, in order to meet the above $P_{loss,\ tot}$ QoS requirement. The following simulation results have been obtained with simulations of 300 s repeated 10 times for each point in order to achieve reliable results.

Figure 8 shows the layer 3 performance results in terms of P_{drop} and $P_{loss,\ tot}$ as a function of the number of SIF video sources per cell with 50 Web traffic flows. In this graph, EDF, PF and PF-ER techniques have been compared. The video SIF sources have a mean bit-rate of 160 kbit/s (PDA scenario) and the Web sources have a mean bit-rate of 5.83 kbit/s. From these results we can note that:

- P_{drop} sensibly increases with the number of video UE's.
- The PF-ER scheme achieves the best performance for the video traffic management, that is the lowest $P_{loss,\ tot}$ value. While, the PF technique is the best solution for the Web traffic performance in terms of the $Delay_{Web}$ parameter. The PF scheme selects the UE for transmissions considering to distribute resources fairly among them so that also Web sources have a good share of resources. While, the PF-ER technique bases its decisions also on deadlines, so that when the system becomes congested (i.e., more resources are used) such approach permits to take better account of the urgency of video packets.
- With the PF-ER scheme we can fulfill the requirement of $P_{loss,\ tot} \leq 7\%$ with 10 video SIF UE's/cell.
- In terms of video traffic management ($P_{loss,\ tot}$) this graph shows that EDF outperforms PF, meaning that it is important to schedule traffic taking into account deadlines rather than exploiting capacity by means of the knowledge of the channel. Other simulation results, not shown here, have shown opposite results in the presence of a lower number of Web traffic sources producing heavier traffic loads: in this case, Web

traffic sources produce more traffic so that there is more congestion and the PF scheme can outperform EDF for the video traffic management.

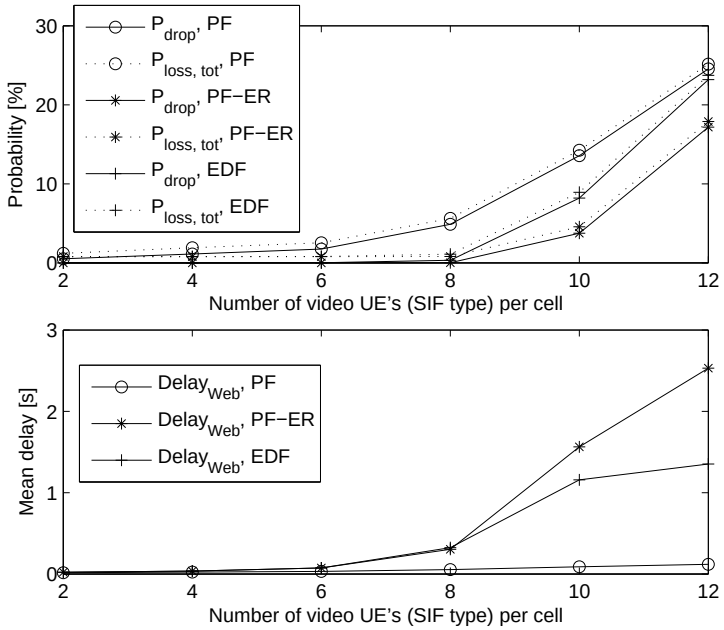

Figure 8: P_{drop}, $P_{loss,\ tot}$ and $Delay_{Web}$ results for the EDF, PF and PF-ER scheduling schemes as a function of the number of video SIF UE's/cell for 50 Web UE's/cell.

Figure 9 shows the layer 3 performance results in terms of P_{drop} and $P_{loss,\ tot}$ as a function of the number of QCIF video sources per cell with 50 Web traffic flows. In this graph, EDF, PF and PF-ER techniques have been compared. Each video QCIF source generates a mean bit-rate of 44 kbit/s (cell-phone scenario) and each Web source has a mean bit-rate of 5.83 kbit/s. From these results we can again note that the PF-ER scheme achieves the best performance for the video traffic management, thus attaining a capacity of 38 video UE's per cell.

Finally, a last block of simulations has been carried out to compare the performance of different scheduling schemes with either adaptive CQI (use

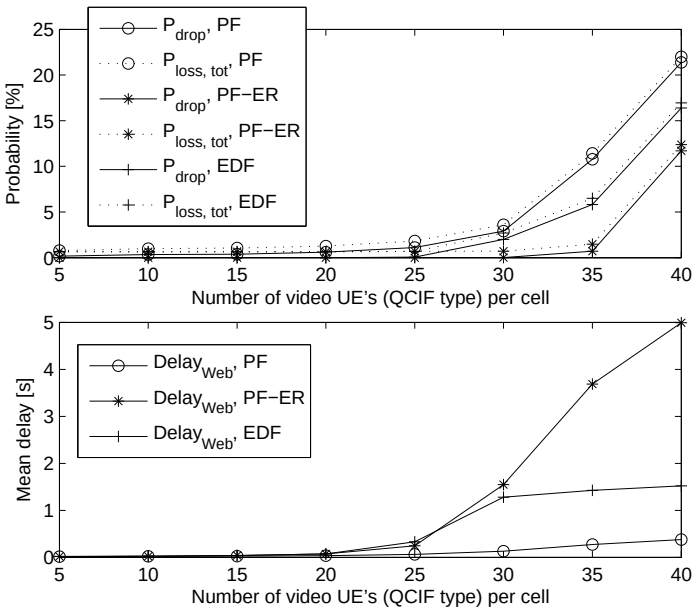

Figure 9: P_{drop}, $P_{loss,\ tot}$ and $Delay_{Web}$ results for the EDF, PF and PF-ER scheduling schemes as a function of the number of video QCIF UE's/cell for 50 Web UE's/cell.

of a feedback channel) or fixed CQI value (no adaptation). Our aim is to evaluate the impact of RTPD on the effectiveness of adaptation in the presence of a rapidly changing channel, like the one for mobile users. In performing this study, we have also considered a scheme where the CQI selection is made on the basis of a channel estimation. We adopt a channel estimation scheme whose performance can be modeled by the probability p that it correctly predicts the SNIR value that the UE will experience when the packet (with the selected CQI at time t) will be received, $SNIR(t + RTPD)$. In other words, the SNIR value used at time t for determining the current CQI value from (4), $SNIR_u(t)$, is determined according to the following model:

$$SNIR_u(t) = (1 - p) \times SNIR(t) + p \times SNIR(t + RTPD)$$

where we have considered $p = 0.6$, which has been *a-posteriori* calculated by using the stochastic channel estimation approach detailed in [23] with the channel trace described in sub-Section in 2.1.

The advantage of the S-HSDPA system with channel estimation is that we can use a lower $h = 1.5$ dB value to fulfill our BLER requirement, thus achieving a higher capacity and a lower P_{drop} value. Figure 10 shows the $P_{loss,\ tot}$ performance for EDF, PF and PF-ER scheduling schemes for different numbers of SIF video UE's and with 50 Web UE's for the following different cases:

- F1 = non-adaptive scheme with fixed CQI = 15;
- F2 = non-adaptive scheme with fixed CQI = 17;
- F3 = non-adaptive scheme with fixed CQI = 20;
- A1 = the adaptive CQI selection scheme considered so far;
- A2 = enhanced scheme with adaptive CQI selection depending on channel estimation.

The results in Figure 10 permit to highlight that, among the non-adaptive schemes, CQI = 17 (i.e., case F2) is the best choice in terms of $P_{loss,\ tot}$. Reducing CQI (i.e., case F1) causes a lower capacity and, hence, P_{drop} increases and, then, also $P_{loss,\ tot}$ is high; while, increasing CQI (i.e., case F3) allows a better capacity, but higher packet losses due to the channel with a consequently high $P_{loss,\ tot}$ value. We can note that the adaptive scheme A1 outperforms the best fixed CQI scheme F2 only for very high traffic loads per cell. In order to support the need of adaptivity with the use of a feedback channel, we envisage here also the adaptive scheme A2 where CQI is selected on the basis of a channel prediction. All the scheduling techniques improve their performance with the A2 scheme; in particular, the PF-ER

scheme achieves the lowest $P_{loss,\ tot}$ value. In conclusion, these results prove that adaptive schemes are motivated in the satellite scenario since they permit to achieve a higher capacity, especially if adaptation is combined with channel estimation. For the studies carried out in the following Section, we still refer to the A1 adaptivity case; further results on the A2 technique are left to a future study.

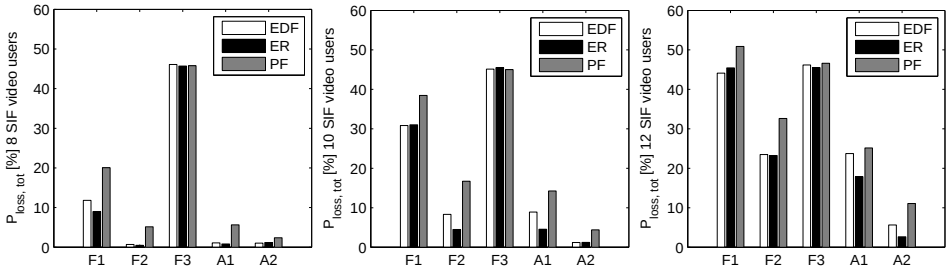

Figure 10: Comparison of non-adaptive and adaptive CQI selection schemes for different scheduling schemes in the presence of different number of video SIF UE's/cell and 50 Web UE's/cell.

6 Evaluation of Objective Video Quality

This Section deals with an almost complete multi-layer study where the resulting performance at the application layer is evaluated in terms of suitable quality parameters. For this purpose we have considered the most common objective video quality indicator, i.e., the *Peak Signal-to-Noise Ratio* (PSNR); in addition to PSNR, also other parameters have been considered in this study, as shown in Table 2.

We have used the video traces previously encoded with Quicktime 7.0 Pro and streamed with *Darwin Streaming Server* (DSS). DSS is the open source version of Apple's QuickTime Streaming Server technology that permits to send streaming media to clients using the industry standard RTP

and *Real Time Streaming Protocol* (RTSP) protocols. The DSS is built on a core server that provides state-of-the-art QoS features and support for the latest digital media standards. Furthermore, DSS provides full compatibility with Quicktime encoder. The streamed packets have been used as input to the S-HSDPA simulator: they have been scheduled and transmitted. Thus, the received video stream is affected by packet losses due to deadline expirations and channel errors. The received stream was played with Video Lan Player 0.8.6. The video has been captured for further video quality analysis in terms of PSNR:

$$PSNR = 10 \times \log_{10} \frac{255^2}{MSE} \tag{15}$$

where MSE is the *Mean Square Error* evaluated as

$$MSE = \frac{1}{l \times m} \sum_{i=1}^{l} \sum_{j=1}^{m} [Orig(i,j) - Deg(i,j)]^2 \tag{16}$$

and where $Orig(i, j)$ denotes the original value of the (i, j) pixel and $Deg(i, j)$ is the received value of the (i, j) pixel for a given video frame.

We have compared the resulting video quality that we obtain at the application level for the video traffic traces transmitted through the S-HSDPA air interface. In this study, we have only considered video traffic flows (i.e., no mixed traffic scenarios) of either QCIF or SIF types. In these circumstances, EDF becomes equivalent to the trivial FIFO case and PF is quite close to PF-ER that, however, takes also into account the residual packet lifetime. This is the reason why we focus the following study only on EDF and PF schedulers. We will also provide some initial considerations related to the PF-ER scheduler; further results for the PF-ER case will be the subject of a future study.

6.1 Cell-phone Scenario Results

In this study, the PSNR values have been clipped to 92.17 dB, in case of error-free frame in error-prone channel. This PSNR clipping value corre-

sponds to one error in one color in one frame resolution. Such clipping has been used, because we need to avoid infinity PSNR values resulting for zero MSE in (16). The PSNR values for single frames of the investigated sequences have been visualized like empirical histograms. This visualization allows us to see the distribution of visible and invisible impairments. According to our empirical experiences, we set the threshold between visible and invisible impairments at PSNR = 36 dB. We have assumed that the frame degradations higher than 36 dB are almost invisible for human visual systems.

Figures 11 and 12 show the PSNR distribution obtained respectively with the EDF scheme and the PF one in the presence of 35 concurrent video sources (QCIF resolution, mean bit-rate of 44 kbit/s). Let us consider the QCIF results shown in Table 2. The mean PSNR value for the whole sequence with PF increases of 3.47 dB with respect to EDF. Moreover, with PF there are 51.74% error-free frames and 61.27% of frames with invisible impairments (behind 36 dB threshold). Furthermore, results obtained with EDF highlight a stronger video degradation: 25.36% error-free frames and 33.03% frames with invisible impairments (behind 36 dB threshold).

6.2 PDA Scenario Results

In this case, the PSNR values have been clipped to 96.98 dB, in case of error-free frame in error-prone channel. This PSNR clipping value corresponds to one error in one color in one frame resolution.

Figures 13 and 14 show the PSNR distribution obtained with EDF and PF in the presence of 12 concurrent video sources (SIF resolution, mean bit-rate of 160 kbit/s). Let us refer to the SIF results shown in Table 2. The mean PSNR value for the whole sequence with PF increases of 3.24 dB with respect to EDF. With PF, we have obtained 41.31% error free-frames and 46.75% frames with invisible impairments (behind 36 dB threshold). Fur-

thermore, a critical video degradation is obtained with EDF: 4.88% error-free frames and 9.59% frames with invisible impairments (behind 36 dB threshold).

Table 2: Video quality results and comparisons in different scenarios.

	EDF		**PF**	
Scenario	QCIF	SIF	QCIF	SIF
$P_{loss,\ tot}$ [%]	7.5%	7.5%	4.7%	7.7%
Mean PSNR [dB]	13.62	12.89	17.10	16.13
Error-free frames [%]	25.36%	4.88%	51.74%	41.31%
Invisible impairments [%]	33.03%	9.59%	61.27%	46.75%

Even if Table 2 highlights that the different scheduling scheme achieve close $P_{loss,\ tot}$ results, the IP packet losses have not the same distributions and these differences have a crucial impact on the video quality. In conclusion, the EDF scheme does not permit a satisfactory video quality and PF scheduler seems a better solution. Moreover, early studies for the above scenario confirm that the PF-ER scheme has a close performance to the PF technique, especially in the QCIF case. A significant performance improvement could be achieved if the IP packet scheduler could be designed to be content-aware; since a loss in an I frame has a greater impact on video quality than losses for other types of video frames, it would be very important that I frames be prioritized by the scheduler. A further study of this topic as well as a detailed investigation of the PF-ER case or its modifications are left to a future study.

7 Conclusions

This paper has investigated the extension of the terrestrial HSDPA to a GEO-based satellite scenario to provide broadband multimedia applications

to mobile users. We have employed suitable channel traces and analytical characterizations relating channel, PHY and transport channel (MAC-hs) performance. EDF, PF and PF-ER schedulers have been considered to manage the transmissions on the HS-DSCH transport channel in the presence of video streaming and Web downloading traffic flows. Referring to the multi-code operation mode, we have evaluated the number of QCIF or SIF video traffic flows that can be supported with adequate QoS requirements in terms of BLER and total packet loss probability, $P_{loss,\ tot}$. The PF-ER scheme permits to achieve the best performance for the time-critical video traffic in the presence of a mixed traffic scenario.

Finally, objective video quality estimations have been carried out on the received video stream with both QCIF and SIF resolutions highlighting that schemes based on the proportionally fair approach permit to achieve better results. The obtained results demonstrate that the simple urgency-based EDF scheme does not permit to achieve an acceptable video quality.

A further work is needed to investigate the impact of retransmissions on the Web traffic performance and the study of cases where more than one UE per TTI is allowed to transmit. Finally, a future study is also needed to deepen the application level performance of the PF-ER scheme and to investigate cross-layer content-aware packet schedulers for video streaming traffic.

Acknowledgments

This paper has been carried out within the framework of the European SatNEx II (contract No. IST-027393), network of excellence, www.satnex.org, joint activity ja2330. The authors thank Prof. Markus Rupp from Vienna University of Technology for supporting their research collaboration.

References

[1] 3GPP, "High Speed Downlink Packet Access; Overall UTRAN Description", *TR 25.855*, Release 5.

[2] H. Holma and A. Toskala. *WCDMA for UMTS: Radio Access for Third Generation Mobile Communications.* Second edition, John Willey & Sons Ltd, 2002.

[3] T. E. Kolding, K. I. Pedersen, J. Wigard, F. Frederiksen, P. E. Mogensen, "High Speed Downlink Packet Access: WCDMA Evolution", *IEEE Vehicular Technology Society News*, Vol. 50, No. 1, pp. 4-10, February 2003.

[4] ETSI, "Satellite Earth Stations and Systems (SES); Satellite Component of UMTS/IMT2000; G-family; Part 1: Physical Channels and Mapping of Transport Channels into Physical Channels (S-UMTS-A 25.211)", *TS 101 851-1.*

[5] ETSI, "Satellite Earth Stations and Systems (SES); Satellite Component of UMTS/IMT2000; G-family; Part 2: Multiplexing and Channel Coding (S-UMTS-A 25.212)", *TS 101 851-2.*

[6] ETSI, "Satellite Earth Stations and Systems (SES); Satellite Component of UMTS/IMT2000; G-family; Part 3: Spreading and Modulation (S-UMTS-A 25.213)", *TS 101 851-3.*

[7] ETSI, "Satellite Earth Stations and Systems (SES); Satellite Component of UMTS/IMT2000; G-family; Part 4: Physical Layer Procedures (S-UMTS-A 25.214)", *TS 101 851-4.*

[8] G. Giambene, S. Giannetti, C. Párraga Niebla, Michal Ries, "Video Traffic Management in HSDPA via GEO Satellite", *in Proc. of the International Workshop on Satellite and Space Communications* (IWSSC 2006), September 14-15, 2006, Leganés, Spain.

[9] L. E. Braten, T. Tjelta, "Semi-Markov Multistate Modeling of Land Mobile Propagation Channel for Geostationary Satellites", *IEEE Transactions on Antennas and Propagation*, Vol. 50, No. 12, December 2002.

[10] K. Lim, S. Kim, "Downlink Radio Resource Allocation for Multibeam Satellite Communications", *IEE Electronics Letters*, Vol. 39, No. 11, pp. 871-872, 29 May 2003.

[11] 3GPP, "End-to-end Transparent Streaming Service; Protocols and Codecs", *TS 26.234*.

[12] M. Ries, O. Nemethova, M. Rupp, "Reference-Free Video Quality Metric for Mobile Streaming Applications", *in Proc. of the DSPCS 05 & WITSP 05*, pp. 98-103, Sunshine Coast, Australia, December 2005.

[13] 3GPP, "End-to-end Transparent Streaming Service; General Description", *TS 26.233*.

[14] O. Nemethova, M. Ries, M. Zavodsky, M. Rupp, "PSNR-Based Estimation of Subjective Time-Variant Video Quality for Mobiles", *in Proc. of the MESAQUIN*, Prague, Czech Republic, June 2006.

[15] A. H. Aghvami, A. E. Brand, "Multidimensional PRMA with Priorized Bayesan Broadcast", *IEEE Transactions on Vehicular Technology*, Vol. 47, pp. 1148-1161, 1998.

[16] 3GPP, "Physical Layer Procedure (FDD)", *TS 25.214*, 2004.

[17] F. Brouwer, I. de Bruin, J. Carlos Silva, N. Souto, F. Cercas, A. Correia "Usage of Link-Level Performance Indicators for HSDPA Network-Level Simulations in E-UMTS", *in Proc. of ISSSTA2004*, Sydney, Australia, 30 August - 2 September 2004.

[18] ETSI "Satellite Earth Stations and Systems (SES); Broadband Satellite Multimedia Services and Architectures; QoS Functional Model", *TS 102 462*-Draft, January 2006.

[19] T. Kolding, "Link and System Performance Aspects of Proportional Fair Scheduling in WCDMA/HSDPA", *in Proc. of the IEEE VTC-Fall 2003*, October 4-9, 2003, Orlando, Florida, USA.

[20] J. T. Entrambasaguas, M. C. Aguayo-Torres, G. Gomez, J. F. Paris, "Multiuser Capacity and Fairness Evaluation of Channel/QoS Aware Multiplexing Algorithms", *4-th COST 290 MCM*, Wurzburg, October 13-14, 2005.

[21] 3GPP, "Transparent end-to-end Packet Switched Streaming Service (PSS)", *TR 26.937*.

[22] O. Casals, C. Blondia, "Performance Analysis of Statistical Multiplexing of VBR Sources", *in Proc. of INFOCOM'92*, pp. 828-838, 1992.

[23] M. T. Wasan. *Stochastic Approximation. Cambridge Tracts in MAthematics and Mathematical Physics*. Ed. J. F .C. Kingman. Vol. I. 1969, Cambridge: Cambridge University Press.

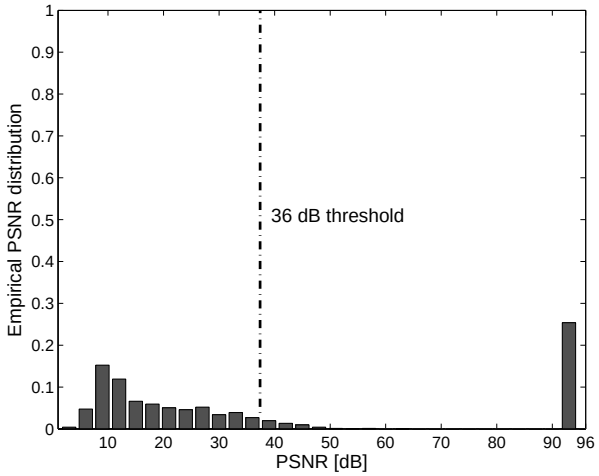

Figure 11: The empirical PSNR distribution for the cell-phone scenario (QCIF) with EDF scheduling.

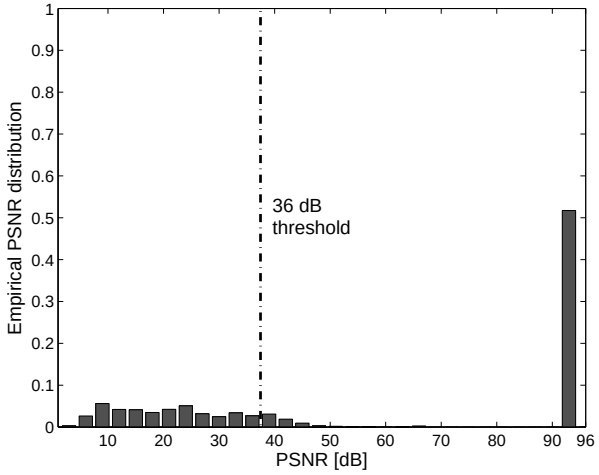

Figure 12: The empirical PSNR distribution for the cell-phone scenario (QCIF) with PF scheduling.

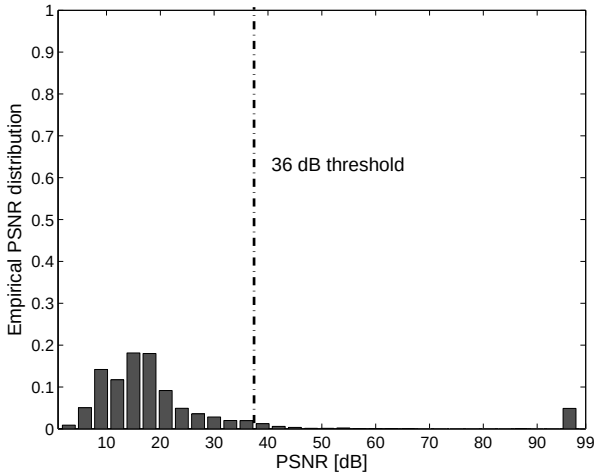

Figure 13: The empirical PSNR distribution for the PDA scenario (SIF) with EDF scheduling.

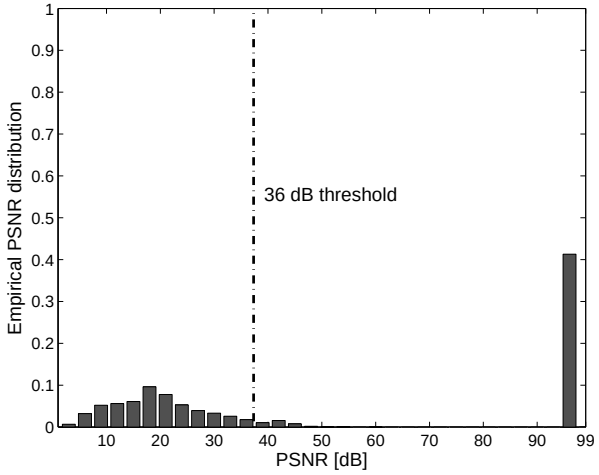

Figure 14: The empirical PSNR distribution for the PDA scenario (SIF) with PF scheduling.